Dynamics of vibrational chaos and entanglement in triatomic molecules: Lie algebraic model*

Zhai Liang-Jun(翟良君), Zheng Yu-Jun(郑雨军)†, and Ding Shi-Liang(丁世良)

School of Physics, Shandong University, Jinan 250100, *China*

(Received 7 January 2012; revised manuscript received 20 February 2012)

In this paper, the dynamics of chaos and the entanglement in triatomic molecular vibrations are investigated. On the classical aspect, we study the chaotic trajectories in the phase space. We employ the linear entropy to examine the dynamical entanglement of the two bonds on the quantum aspect. The correspondence between the classical chaos and the quantum dynamical entanglement is also investigated. As an example, we apply our algebraic model to molecule H_2O.

Keywords: dynamical entanglement, classical chaos, intramolecular vibration, H_2O

PACS: 05.45.Ac, 05.45.Mt, 33.20.Tp, 03.67.Mn **DOI:** 10.1088/1674-1056/21/7/070503

1. Introduction

As a potential quantum resource for applications in quantum computation and quantum information, entanglement has triggered enormous efforts to understand its dynamical properties in various systems.[1−3] Besides those theoretical models, the dynamical entanglement of realistic polyatomic molecular systems has emerged as an exciting research topic recently.[4−7] It is suggested that the vibrational states of polyatomic molecules can be used to represent the qubits, and the shaped femtosecond laser pulses in the infared (IR) regime can be used to implement the quantum logic operation.[8,9] The number of available qubits is proportional to the number of vibrational degrees of freedom when the molecular vibrational states are used as the qubit base, and it is demonstrated that a quite high quantum gate fidelity can be realized.[9] Since the entanglement plays an important role in quantum information and quantum computation, the study of the dynamical entanglement in a realistic molecular system is interesting.

On the other hand, decoding the dynamical information hidden in the frequency domain spectrum can be traditionally studied via the classical–quantum approach,[10−15] which provides us with a vivid picture of the intramolecular motion. A natural way for this is probably to study the classical phase structures,[16−19] and there is sufficient evidence that the information from the classical analysis is comparable with the corresponding quantum phenomena.[20−22] Using this method, some interesting questions have been well studied, such as the bottleneck of intramolecular vibrational energy redistribution (IVR)[23] and the intramolecular chaos of high excited molecules.[24−27] Meanwhile, it is demonstrated that the intramolecular vibration is chaotic when the system is in the highly excited state, even for the simple triatomic systems.[14−16] And the studies of the intramolecular chaos have shown that the chaos plays an important role in IVR,[28] assigning the vibrational spectra,[20] and the coherent control of the intramolecular process.[29] The Poincaré section and the Lyapunov exponent are two useful tools in such investigations. The Poincaré section technique is used to reduce the dimensions of the system, by means of which one can observe the classical phase structure directly. And the Lyapunov exponent is a parameter to detect whether the system is chaotic or not.

The classical–quantum correspondence in molecular systems has been investigated via many pathways, such as the shape of the eigenfunction,[30] the EBK method,[31] and the dynamics in the quantum phase space.[20] Recently, the quantum dynamical entanglement has also been studied to investigate the classical–quantum correspondence. Studies on many systems have shown that the dynamical entanglement produc-

*Project supported by the National Natural Science Foundation of China (Grant Nos. 91021009 and 10874102) and the National Basic Research Program of China (Grant No. 2009CB929404).

†Corresponding author. E-mail: yzheng@sdu.edu.cn

© 2012 Chinese Physical Society and IOP Publishing Ltd

tion can be an indication of the underlying classical chaos.[32−34] One of the important properties obtained in those studies illustrates that the dynamical entanglement is the largest when the initial state lies at the edges of the regular islands or in the chaotic sea.[35] The correspondence between the (dynamical) entanglement and the vibration provides us with a new way to explore the intramolecular dynamics, and helps us to understand the mysteries of the dynamical entanglement. The triatomic systems, as the most simple polyatomic molecules, serve as the prototype to develop theories and to understand new phenomena of the intramolecular dynamics, such as the normal and the local mode behaviors of H_2O molecule and the transition between them,[16] the dynamics of energy transfer between bonds both from the classical and the quantum viewpoints for the ABA molecule,[36,37] and the chaos.[13−17] In this paper, we focus our attention on the classical dynamics of molecular vibrations and the dynamical entanglement in the triatomic molecule. We use the Lie algebraic model. We also analyze the correspondence between the classical dynamics of molecular vibrations and the dynamical entanglement. We expect that this work can be helpful to understand the dynamical entanglement in molecular systems and provide a new viewpoint for quantum computation using the molecular vibrations.

The Lie algebraic theory of molecules is an effective approach to describe the molecular vibrations and rotations in polyatomic molecules.[38−43] This method has a simple form in the description of a molecular Hamiltonian, and the anharmonicity of each mode and the resonances between different modes are introduced automatically by the matrix elements of the corresponding group operators.[44] Because of these advantages, the algebraic method has extensive applications in small molecules and molecular chains to study many questions,[45] such as vibrational energy levels, potential energy surfaces, dynamical entanglement of vibrations, and multiphoton selective excitation.[38−41,46,47] Meanwhile, the classical limit of the Lie algebraic Hamiltonian can be directly obtained by calculating the expectation value of the quantum Hamiltonian over the coherent state[39] or using the intensive boson operators introduced by Gilmore.[48] This is helpful for the discussion of the quantum–classical correspondence in the framework of the Lie algebraic model.

The organization of this paper is as follows. In Section 2, the U(4) algebraic Hamiltonian for the triatomic molecules and the theoretical framework of dynamical entanglement are reviewed. And, the classical limit of the U(4) algebraic Hamiltonian is deduced by using the intensive boson operators. In Section 3, the classical phase structures of H_2O are depicted in the Poincaré sections, and the mean Lyapunov exponents are calculated to identify the chaotic degrees of energy levels of H_2O. The dynamical entanglement with the initial states of the Fock and the coherent states is studied using the linear entropy, and the correspondence between the vibrations and the dynamical entanglement is also discussed in this section. A brief summary and outlook are presented in Section 4.

2. Dynamical entanglement and chaos of triatomic molecules

For completeness, we first concisely review the U(4) algebraic model of triatomic molecules. The detail description can be found in Refs. [39] and [42]. The dynamical symmetric chains for a triatomic molecule are expressed as[39]

$$\begin{aligned} &\mathrm{U}_1(4)\otimes\mathrm{U}_2(4)\supset\mathrm{U}_{12}(4)\supset\mathrm{O}_{12}(4),\\ &\mathrm{U}_1(4)\otimes\mathrm{U}_2(4)\supset\mathrm{O}_1(4)\otimes\mathrm{O}_2(4)\supset\mathrm{O}_{12}(4). \end{aligned} \quad (1)$$

The quantum Hamiltonian, in terms of linear Casimir and Majorana operators of subgroups, for group chains (1) is written as

$$H = A_1C_1 + A_2C_2 + A_{12}C_{12}^{(1)} + A'_{12}C_{12}^{(2)} + \lambda M_{12}, \quad (2)$$

where A_1, A_2, A_{12}, A'_{12}, and λ are the expansion coefficients, which are determined by fitting the spectroscopic data; C_1 and C_2 are Casimir operators of groups $\mathrm{O}_1(4)$ and $\mathrm{O}_2(4)$, respectively; $C_{12}^{(1)}$ and $C_{12}^{(2)}$ are two Casimir operators of $\mathrm{O}_{12}(4)$; and M_{12} is the Majorana operator denoting the coupling between two bonds. In the local basis $|[N_1][N_2](\omega_1,0)(\omega_2,0)(\tau_1,\tau_2)\rangle$, the matrices of the Casimir operators are diagonal, but the matrix of the Majorana operator has both diagonal and non-diagonal elements. The explicit forms of the matrix elements can be found in Ref. [49].

The algebraic Hamiltonian (2) has been used to investigate the vibrational levels of the triatomic molecules, and it represents the realistic situations of the triatomic molecules. Based on the quantum Hamiltonian of Eq. (2), we investigate the dynamics of dynamical entanglement and chaotic dynamics (in

its classical limits) of the molecules. There are several measures of dynamical entanglement, such as the relative entropy, the entanglement of formation, and the linear entropy. Among them, the linear entropy[4,5] is a simple but widely-used measure of entanglement. It is defined by

$$S_{\rm l} = 1 - {\rm Tr}_1[\rho_1(t)]^2, \tag{3}$$

where ${\rm Tr}_i$ denotes the trace over subsystem i ($i = 1,\ 2$), and

$$\rho_1(t) = {\rm Tr}_2|\psi(t)\rangle\langle\psi(t)|, \tag{4}$$

is the reduced-density matrix, and indexes 1 and 2 represent bonds 1 and 2, respectively. Here $|\psi(t)\rangle$ is the state of the molecular system. Its evolution in time under the action of the Hamiltonian of Eq. (2) is obtained by

$$|\psi(t)\rangle = {\rm e}^{-{\rm i}Ht}|\psi(0)\rangle, \tag{5}$$

where the reduced Planck constant $\hbar$ has been set to 1, and $|\psi(0)\rangle$ is the initial state, which can be selected to be the Fock states or the continuous-variable-type states, such as the coherent states. The detail calculation of dynamical entanglement in molecules can be found in Refs. [4] and [5].

In the coset space of the algebraic structure, we are able to get the classical limit of the quantum algebraic Hamiltonian of Eq. (2). Following the approach using the intensive boson operators, the classical limit of algebraic Hamiltonian (2) is obtained as[39]

$$\mathscr{H}_{\rm cl} = H(z, z^\dagger), \tag{6}$$

where z is a complex quantity, and $z^\dagger$ is its corresponding complex conjugate.

A more familiar form of this Hamiltonian is obtained by considering the canonical coordinates through the canonical transformation[39]

$$\begin{aligned} z_\alpha &= \frac{1}{\sqrt{2}}(q_\alpha + {\rm i}p_\alpha), \\ z_\alpha^\dagger &= \frac{1}{\sqrt{2}}(q_\alpha - {\rm i}p_\alpha), \quad ({\rm i} = \sqrt{-1}), \end{aligned} \tag{7}$$

where (q_α, p_α) ($\alpha = 1, 2$) are the canonical variables in the phase space.

With the above transformation, the classical limit of the algebraic Hamiltonian is of the form

$$\mathscr{H}_{\rm cl} = \mathscr{H}_{\rm cl}(q_1, p_1; q_2, p_2). \tag{8}$$

To describe the chaotic dynamics of molecular vibrations, we need to extract the kinetic and the potential energy contributions from the classical limits of Eq. (8).

The potential energy surface is defined as[39]

$$\mathscr{V}(q_1, q_2) = \mathscr{H}_{\rm cl}(q_1, p_1 = 0, q_2, p_2 = 0). \tag{9}$$

For the sake of our description, we need to transform coordinates q_α to the intramolecular coordinates r_α. This transformation is suggested by the following equation:[39]

$$q_\alpha^2 = {\rm e}^{-\beta_\alpha(r_\alpha - r_{\alpha\,{\rm e}})}, \quad (\alpha = 1, 2), \tag{10}$$

where $r_{\alpha\,{\rm e}}$ is the equilibrium bond length of the bond, and β_α is the spectroscopic parameter. In terms of intramolecular coordinates, the potential function $\mathscr{V}(r_1, r_2)$ in the case of bond angle frozen at its equilibrium position is written as[38,39]

$$\begin{aligned} &\mathscr{V}(r_1, r_2) \\ &= (A_1 + A_{12})N_1^2[2 - {\rm e}^{-\beta_1(r_1 - r_{1{\rm e}})}]\,{\rm e}^{-\beta_1(r_1 - r_{1{\rm e}})} \\ &\quad + (A_2 + A_{12})\,N_2^2[2 - {\rm e}^{-\beta_2(r_2 - r_{2{\rm e}})}]\,{\rm e}^{-\beta_2(r_2 - r_{2{\rm e}})} \\ &\quad + 2A_{12}N_1N_2\big\{[2 - {\rm e}^{-\beta_1(r_1 - r_{1{\rm e}})}]\,{\rm e}^{-\beta_1(r_1 - r_{1{\rm e}})} \\ &\quad \times [2 - {\rm e}^{-\beta_2(r_2 - r_{2{\rm e}})}]\,{\rm e}^{-\beta_2(r_2 - r_{2{\rm e}})}\big\}^{1/2} \\ &\quad + \frac{1}{4}\lambda N_1N_2\{2\,{\rm e}^{-\beta_1(r_1 - r_{1{\rm e}})} + 2\,{\rm e}^{-\beta_2(r_2 - r_{2{\rm e}})} \\ &\quad - 2\,{\rm e}^{-\beta_1(r_1 - r_{1{\rm e}}) - \beta_2(r_2 - r_{2{\rm e}})} \\ &\quad - 2[(2 - {\rm e}^{-\beta_1(r_1 - r_{1{\rm e}})})\,{\rm e}^{-\beta_1(r_1 - r_{1{\rm e}})} \\ &\quad \times (2 - {\rm e}^{-\beta_2(r_2 - r_{2{\rm e}})})\,{\rm e}^{-\beta_2(r_2 - r_{2{\rm e}})}]^{1/2}\}. \end{aligned} \tag{11}$$

The general properties of the potential energy of Eq. (11) were studied in Refs. [38] and [39], and they have been successfully applied to determine the potential energy surfaces for both linear and nonlinear triatomic molecules.[38,39,49–52]

However, it is tricky to extract the kinetic contributions from the classical limit of the algebraic Hamiltonian of Eq. (8). We suggest here that under the Born–Oppenheimer approximation, the kinetics of the triatomic molecules in the internal coordinate system read

$$\mathscr{T} = \sum_{i,j} G_{i,j}p_ip_j, \qquad (i, j = 1, 2, 3), \tag{12}$$

where p_1 and p_2 are the momenta corresponding to the stretching vibrations of the two bonds, and p_3 is the momentum of the bending vibration. In this paper, we assume that the bond angle is frozen at its equilibrium position. For the triatomic molecules, following Wilson *et. al.*,[53] we obtain the kinetic matrix

$$G_{11} = \frac{1}{2}(\mu_1 + \mu_2), \quad G_{12} = \frac{1}{2}\mu_3\cos\phi_0,$$

$$G_{21} = \frac{1}{2}\mu_3 \cos\phi_0, \quad G_{22} = \frac{1}{2}(\mu_2 + \mu_3), \quad (13)$$

where $\mu_1 = 1/m_1$, $\mu_2 = 1/m_2$, m_1 and m_2 are the masses of the atoms at the two ends of the bonds; $\mu_3 = 1/M$, and M is the mass of the central atom; and ϕ_0 is the equilibrium bond angle. The kinetic energy (12) is rewritten as

$$\begin{aligned}\mathscr{T}(p_1, p_2) = & \frac{1}{2}[(\mu_1 + \mu_3)p_1^2 + (\mu_2 + \mu_3)p_2^2] \\ & + \mu_3(\cos\phi_0)p_1 p_2. \end{aligned} \quad (14)$$

The classical Hamiltonian in the case of frozen bond angle, by adding Eqs. (11) and (14), is written as

$$\mathscr{H}_{\rm cl}(r_1, r_2, p_1, p_2) = \mathscr{T}(p_1, p_2) + \mathscr{V}(r_1, r_2). \quad (15)$$

The canonical coordinates (r_1, r_2) and momenta (p_1, p_2) satisfy Hamilton's canonical equations[16]

$$\begin{aligned}\frac{{\rm d}r_\alpha}{{\rm d}t} &= \frac{\partial \mathscr{H}_{\rm cl}}{\partial p_\alpha}, \\ \frac{{\rm d}p_\alpha}{{\rm d}t} &= -\frac{\partial \mathscr{H}_{\rm cl}}{\partial r_\alpha}, \quad (\alpha = 1, 2). \end{aligned} \quad (16)$$

In order to obtain the chaotic dynamics in the molecular vibrations of Hamiltonian in Eq. (15), we numerically integrate Hamiltonian Eq. (16).

3. Results and discussion

In this section, the dynamics of vibrational chaos and the dynamical entanglement of the typical triatomic molecule H_2O are studied using the theoretical framework developed in the previous section. The parameters in Eqs. (2) and (15) for molecule H_2O taken from Refs. [38] and [39] are listed in Table 1. Parameters N_i, A_i, r_{ei}, and β_i describe the vibrations in bond i of the molecule, and A_{12}, λ are the parameters representing the interacting term between two bonds in the molecule. The ϕ_0 is the bond angle at the equilibrium. The parameters in Table 1 can represent the vibrational natures of triatomic molecule H_2O, since they have been testified in the study of vibrational levels, potentials, etc.[38–40]

Table 1. Parameters for triatomic H_2O, where $i = 1$ and 2 indicate the two bonds in the molecule.

Molecule	N_i	β_i/Å^{-1}	A_i/cm^{-1}	A_{12}/cm^{-1}	λ/cm^{-1}	r_{ei}/Å
H_2O	42	2.354	−18.2219	−2.85	1.0571	0.9706

3.1. Chaotic dynamics of H_2O

The Poincaré sections in this paper are defined as the surfaces upon bond 2 at its equilibrium position with a positive momentum. Our calculations show that the vibrations of molecule H_2O are (quasi-) periodic when the total vibrational energy (TVE) is lower than 33000 cm^{-1}. The corresponding Poincaré sections are plotted in Fig. 1. Panel (a) of Fig. 1 shows the section of TVE = 3660.1 cm^{-1}, and the corresponding quantum state is $|0, 1\rangle$. This section is composed of two tori bundles of regular motions: the lower region represents the antisymmetric normal mode and the quasi-periodic motion around it; the upper bundle is composed of two jointed islands, which represent the local mode motions and the invariant tori around them. For the normal mode vibration, the energy freely exchanges between the two bonds. However, for the local mode vibration, once one bond is excited, the energy of the bond remains in that bond. Thus, the island close to the center of the section represents the local motion in which the energy of bond 1 is lower than that of bond 2, and the other island is the local mode vibration in which the energy of bond 1 is larger than that of bond 2. We name the latter local mode 1, meanwhile the former is named local mode 2. Besides these local mode islands, the invariant tori around the two islands have the character of symmetric normal mode motion, where TVE is almost averaged to those of the OH bonds. Due to the weak coupling between these two OH bonds, it is not surprising that the local mode tori appear in this section.

With the increase of TVE, the local mode regions occupy more and more space in the Poincaré section. In panel (b) of Fig. 1, we show the Poincaré section of TVE = 7204.40 cm^{-1}. Its corresponding quantum state is $|0, 2\rangle$. In this case, the region of local mode 1 deforms into the shell part of the section. Meanwhile, the region of local mode 2 shrinks into the yolk part. In addition, the energy discrepancies for the local mode tori are also increasing with the TVE. Based on our calculation, we also find that the two OH bonds vibrate in the domain of (1:1) resonance. Such a phenomenon means that the energy discrepancy of the local mode motion is not high enough to cause a frequency discrepancy. Thus, a normal mode description is suitable for H_2O in this low TVE range.

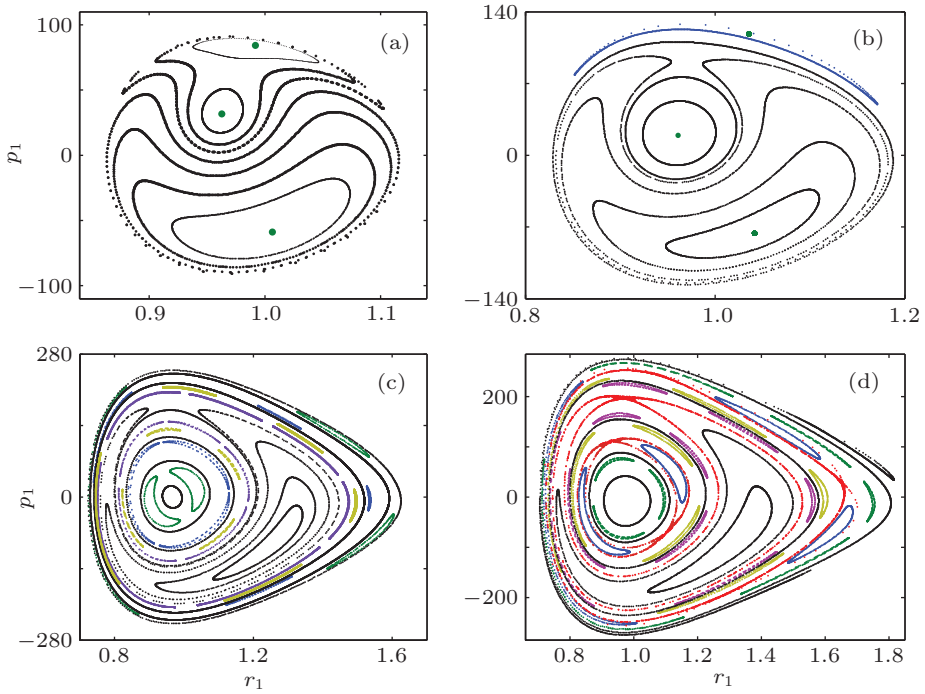


Fig. 1. (colour online) Poincaré sections of H_2O molecule. Panels (a), (b), (c), and (d) show the Poincaré sections of TVE = 3660.0 cm^{-1}, 16901.1 cm^{-1}, 27700.4 cm^{-1}, and 33752.0 cm^{-1}, respectively. In panel (c), the resonance islands of (2 : 3) ((3 : 2)), (3 : 4) ((4 : 3)), (4 : 5) ((5 : 4)) and (5 : 6) ((6 : 5)) are labeled using green, blue, yellow, and violet colours, respectively. The chaotic trajectories in panel (d) are labeled using red colour.

The normal mode vibrations are not the whole story of the H_2O molecule. The breakdown of this description arises with the appearance of resonance zones in the Poincaré section. A resonance zone is easily detected as a chain of islands.[54] The tori bundle in the islands is an $(n : m)$ periodic torus and quasi-periodic tori around it, where $(n : m)$ is used to denote the ratio of the bond vibrational frequencies. The resonance zones firstly appear in the Poincaré section when TVE is around 20000 cm^{-1}, and the corresponding total vibrational quantum number is about 6. We display one typical section of TVE = 27700.4 cm^{-1} with quantum state $|8, 0\rangle$ in Fig. 1(c). There are eight distinct resonance zones labeled with different colours in the figure: (3 : 2), (4 : 3), (5 : 4), and (5 : 6) resonance zones locate in the yolk part; and the resonance zones of (6 : 5), (4 : 5), (3 : 4), and (2 : 3) belong to the shell. Due to the symmetry of the molecule, resonances $(n : m)$ and $(m : n)$ have the same physical properties, and they are labeled with the same colour in the section. Moreover, the classical nonlinear resonance is an important phenomenon in the intramolecular dynamics, and the recent studies[28] show that the resonance could be a resource of the dynamical tunneling.

Since the number of the resonance islands grows with TVE, we can not always study the single resonance behavior, especially in the high excited states. According to the conjecture of Chirikov,[55] the overlapping of resonances could be a route to the chaotic motion. In Fig. 1(d), we give the surface of TVE = 33752.00 cm^{-1} of quantum state $|10, 0\rangle$. We find that the irregular motion appears firstly in the boundaries of the normal mode and the resonance zones of (2 : 3) and (3 : 2) (labeled with red colour). Because the resonance overlapping is not very strong at this TVE, the soft chaotic trajectories only occur in the slim regions close to the separatrix. However, with TVE increasing further, a single resonance zone as well as the overlapping resonance zone expands its area, which leads to the appearance of strong chaotic trajectories.

To describe the chaotic dynamics, the Lyapunov exponent (LE) is widely used. For one trajectory in the n-dimensional space, the corresponding LE is defined as the average exponential rate of the divergence from its initially nearby trajectories. One trajectory in the n-dimensional space possesses n LEs, and the maximum one is usually taken as an indicator to detect whether the trajectory is chaotic or not. The chaotic degree of a fixed TVE is signed by the mean value of LEs (MLE) of the classical trajectories. To present these characters of molecule H_2O, we calcu-

late the MLE of 100 tori for a fixed TVE. The MLE as a function of TVE is shown in Fig. 2. The figure shows that the chaotic degree obtains its maximum value when TVE is around the dissociation energy of single bond D_{ei} $(i = 1, 2)$. In the algebraic model, D_{ei} is expressed as

$$D_{ei} = -(A_i + A_{12})N_i^2, \quad (i = 1, 2). \tag{17}$$

For H_2O molecule, $D_{ei} = 47225.6$ cm^{-1}.

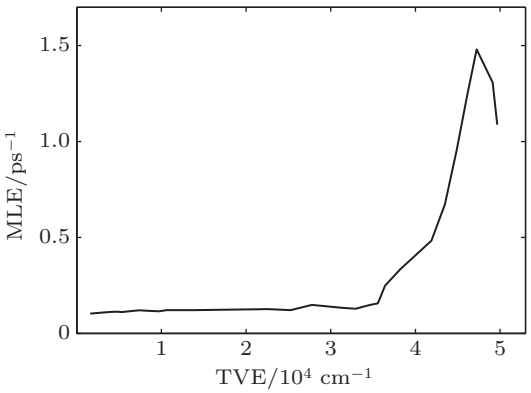


Fig. 2. The MLE as a function of TVE for H_2O.

The Poincaré section of TVE = 46123 cm^{-1} is plotted in Fig. 3(a). Although the surface is dominated by the chaotic trajectories, the chaotic trajectories are always confined by the resonance islands and the invariant tori. The most chaotic trajectories are located at both the inner part of the yolk and the border of the shell. These trajectories correspond to the vibrations of the H_2O molecule with the most part of the TVE located in one bond. Due to the abundant resonance zones in such regions, these chaotic trajectories are in the most chaotic state. The chaos is another way to enhance the dynamical tunneling besides the resonance, and it does have the function to enhance the energy exchange between the bonds.

When TVE transcends the bond's dissociation limit D_{ei}, the inner part of the yolk and the border of the shell of the Poincaré section will have no torus. The blank space (i.e., no torus) is due to that the tori in such regions correspond to the molecular vibrations with one of the OH bonds possessing the energy bigger than its dissociation limit, which causes the dissociation of the H_2O molecule. Figure 3(b) gives the section of TVE = 49671 cm^{-1}, which shows the typical surface of the section with TVE transcending D_{ei}. The most chaotic tori, as shown in Fig. 3(a), are disappeared, correspondingly, the MLE is decreased, which means that with the TVE grows even higher, the vibration draws back to regular.

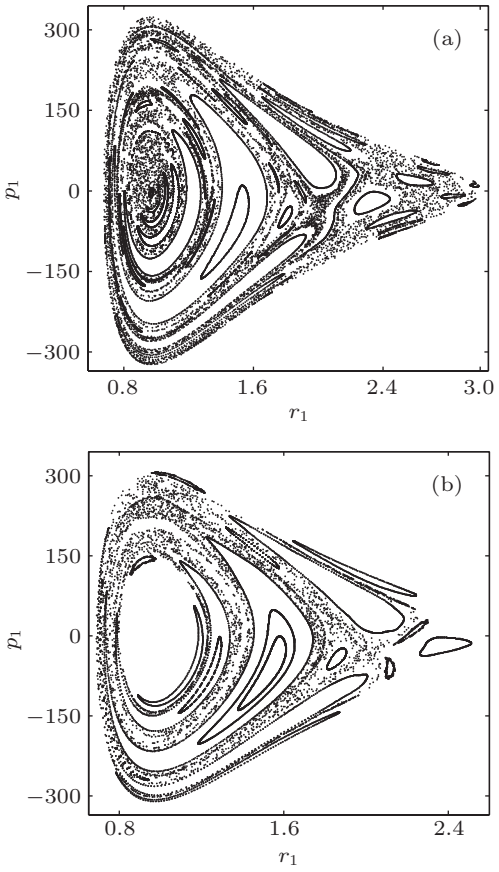


Fig. 3. Poincaré sections of H_2O for (a) TVE = 46123 cm^{-1} and (b) TVE = 49671 cm^{-1}.

3.2. Dynamics of entanglement and its correspondence to chaotic dynamics

A direct method to explore the connections between the dynamical entanglement and the underlying chaotic tori is through preparing an initial coherent state which centers precisely on a point of the Poincaré section. In this paper, however, we employ another viewpoint to describe this. That is, the classical dynamics is employed to understand the characters of the dynamical entanglement of molecule H_2O.

The Fock state has an obvious physical meaning in quantum computation, moreover, the dynamical entanglement of the Fock state is meaningful to understand the intramolecular dynamics. Here, the Fock state is written as

$$|\psi(0)\rangle = |N_1, v_a\rangle \otimes |N_2, N - v_a\rangle \equiv |v_a, N - v_a\rangle, \tag{18}$$

where N is the total quantum vibrational number of the two OH bonds, and v_a is the quantum vibrational number of bond 1. When the Fock state is selected as

the initial state, N is the polyad number during the evolution of the molecular system. Thus, all the states with the same N (namely, states $|0, N\rangle$, $|1, N-1\rangle$, $|2, N-2\rangle$, ..., $|N-1, 1\rangle$, and $|N, 0\rangle$) have their contributions to the evolution of the states considered. The $S_{\rm l}$s of the symmetrical initial Fock states, such as $|v_{\rm a}, N-v_{\rm a}\rangle$ and $|N-v_{\rm a}, v_{\rm a}\rangle$, have an identical shape of evolution.

Figure 4 shows the $S_{\rm l}$s for three Fock sates $|0,1\rangle$, $|0,2\rangle$, and $|1,1\rangle$. In this low energy regime, the classical calculation shows that the bonds are vibrating in the $(1:1)$ resonance, thus the $S_{\rm l}$s vibrate in the stable range and show a neat periodicity. But, as the local mode reflection in the evolution of $S_{\rm l}$, the period of state $|0,2\rangle$ is about twice of that of state $|1,1\rangle$. It should be noticed that the $S_{\rm l}$s of these three Fock states are all oscillating from the disentanglement to their maximum values periodically. Such features make the states usable, since the disentanglement is also necessary for the quantum computation.

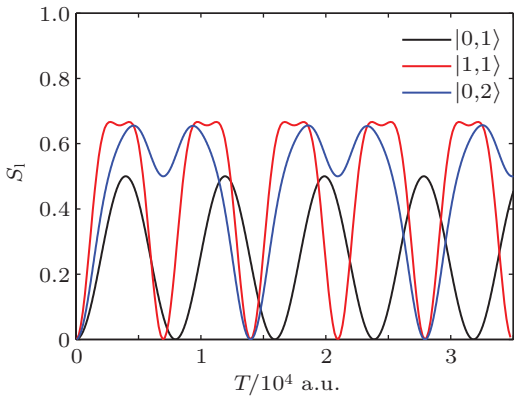


Fig. 4. (colour online) Linear entropies $S_{\rm l}$ as a function of time for different initial states.

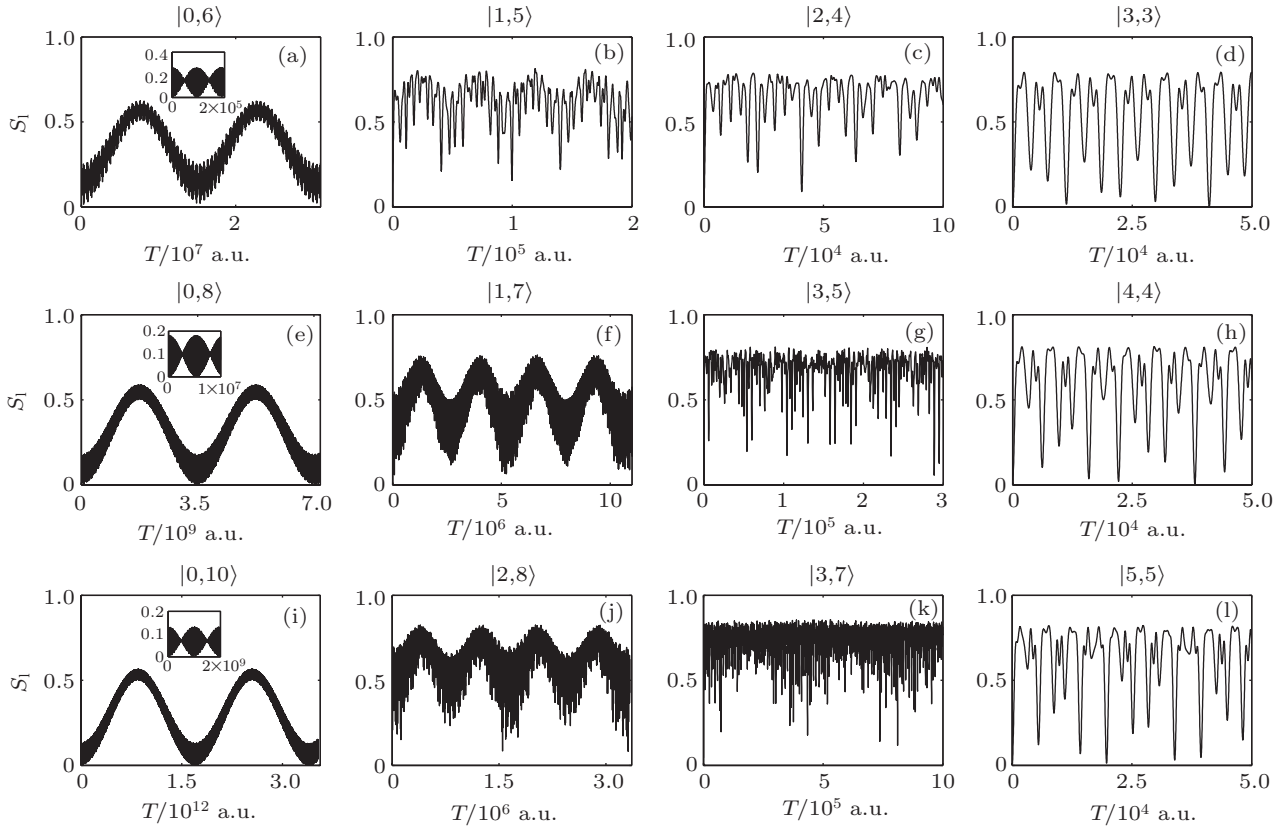


Fig. 5. The $S_{\rm l}$s each as a function of time for the initial states with N being ((a)–(d)) 6, ((e)–(h)) 8, and ((i)–(l)) 10. The packets in the early time are shown in the insets.

Two dynamical features of the local mode molecules are that the local mode vibration exists in various TVE levels and the affection of the local mode will be sustainingly enhanced with the growth of TVE. The enhancement is demonstrated by the increasing energy discrepancy of the two bonds. Correspondingly, the evolution of $S_{\rm l}$ in the case of the initial local mode states shows neat beats. For example, the cases with the initial states of $|0,6\rangle$, $|0,8\rangle$, and $|0,10\rangle$ are displayed in the first column of Fig. 5. All these

time-dependent $S_{\rm l}$s for the initial local mode states are composed of two grades of beats: the packets in the early time (illustrated in the insets of the first column of Fig. 5) and the neat sine wave made up of the packets. The packets can be seen as the impact from the states near the local mode states. The impact from the states far away from the local mode states arises only after a long time evolution. With N growing, the distance between the far away states grows as well, thus the periods of $S_{\rm l}$s for the initial local mode states increase as well. The growing periods of $S_{\rm l}$s are considered as the symbols of the energy discrepancy of the local mode vibration in the classical calculation, in other words, the increasing period of $S_{\rm l}$ is corresponding to the sustaining enhancement of the local mode. The growing periods of these $S_{\rm l}$s for the initial local mode states indicate that the entanglement can last for a long time. The long time sustained entanglement for the local mode state could, therefore, be applied to quantum computation and quantum information.

The Fock states with the same N can be classified into one series to discuss the behavior of the dynamical entanglement when the initial states are varying from local to normal mode states. Every row of Fig. 5, from left to right, displays the $S_{\rm l}$s of the initial local to normal states. When the initial states are changed from local to normal mode states, the beats become inconspicuous, and their corresponding periods decrease as well (notice that the time scales of the panels in Fig. 5 are not the same). Such phenomena are due to the loss of the local mode character, which is analog to the shrinking of energy discrepancy when the classical tori change form local to normal mode regions in the classical mechanical. Furthermore, the maximum values of $S_{\rm l}$ ($S_{\rm lmax}$) are also examined in Fig. 6. It is interesting that the maximum value of $S_{\rm lmax}$s of one series of states is located at the transition states from the local mode to the normal one. The results verify the previous conclusion that the entanglement is the largest when the initial states lie at the junctions of different regions of vibrational modes in the Poincaré section.

Since the classical nonlinear resonances and chaos play an important role in the dynamical tunneling and the elimination of the local mode,[28] we therefore expect that they have influences on the evolutions of $S_{\rm l}$s. We will discuss the detailed functions of the single resonance island and the chaotic trajectory on the entanglement elsewhere, since we need to find the direct correspondence between the initial Fock states, the chaotic trajectories, and the resonance islands exactly. Alternatively, here we explore the global effects of the nonlinear resonances and chaos by employing the following coherent state:

$$|\psi(0)\rangle = {\rm e}^{-|\alpha|^2/2} \sum_n^N \frac{\alpha^n}{\sqrt{n!}} |n, N-n\rangle, \qquad (19)$$

where α is a parameter denoting the amplitude of the coherent state. Here, we set α to be the maximum real number satisfying $\langle\psi(0)|\psi(0)\rangle \approx 1$. The N varies from 1 to 18 (with TVE lower than 50000 cm^{-1}). For a fixed value of N, the coherent state is viewed as the superposition of a series of Fock states. In the TVE range confined by N, this state can be the bridge connecting the quantum and the classical dynamics. The long time-averaged entanglement is an efficient quantity (characteristic parameter) to evaluate the comprehensive effect of the classical local mode vibration, normal mode vibration, resonances, and chaos.[32] Here, we define the long time-averaged entanglement as the average linear entropy $\langle S_{\rm l}\rangle$

$$\langle S_{\rm l}\rangle = \frac{1}{T}\int_0^T S_{\rm l}(t)\,{\rm d}t, \qquad (20)$$

where the evolution time T is set to be 10^8 a.u. Comparing to the relaxation of the molecular vibration, this time is long enough, and many operations can be applied. The variation of $\langle S_{\rm l}\rangle$ with the growing N is plotted in Fig. 7.

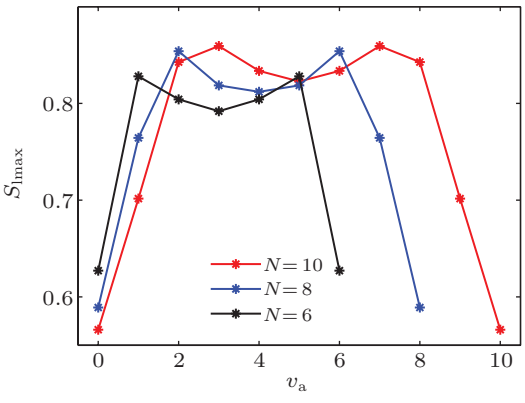


Fig. 6. (colour online) The $S_{\rm lmax}$s of the Fock states with $N = 6$, 8, and 10.

The $\langle S_{\rm l}\rangle$ obtains its first peak at $N = 3$, where the local mode tori begin to occupy a significant proportion of the Poincaré section. Then as N grows, the local mode tori occupy more and more area in the Poincaré section, meanwhile $\langle S_{\rm l}\rangle$ decreases, the correspondence indicates that the local mode vibration is

the main factor that reduces the entanglement. The $\langle S_{\rm l}\rangle$ starts to grow again when $N > 6$, and the resonance islands and the chaotic trajectories begin to appear in the Poincaré section. Despite that the local mode vibration is reinforced, $\langle S_{\rm l}\rangle$ still grows with the increasing N, which shows that the resonances as well as the chaos have the function of enhancing the entanglement between the two stretching bonds.

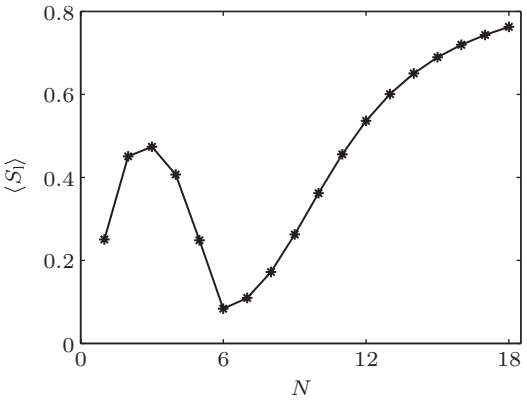


Fig. 7. The $\langle S_{\rm l}\rangle$ of the coherent state as a function of N.

4. Conclusion and outlook

In this paper, the dynamics of H_2O in the case of a frozen bond angle are investigated with the Poincaré section, the LE, and the quantum dynamical entanglement by employing the U(4) algebraic model. Our study shows that when TVE is lower than 33000 $\rm cm^{-1}$ (its corresponding quantum vibrational number is about 10), the vibrations are (quasi-)periodic, and the most chaotic vibration appears when TVE is around the single bond's dissociation limit. In the quantum aspects, we find that the linear entropies show beat phenomena, and their periods increase with the increase of the local mode affection when the Fock states are chosen as the initial states. The largest linear entropies appear when the initial states are chosen to be the transition states from local to normal. When the coherent states are chosen as the initial states, the turning points of the curve of $\langle S_{\rm l}\rangle$ versus N correspond to the changes of the classical vibrational states, i.e., the appearance of resonance. By comparing the classical and the quantum results, we draw the conclusion that the beats in the quantum dynamical entanglement indicate the classical local mode vibration, and the resonance and chaos have the function of enhancing the entanglement production.

The H_2O is a typical local mode molecule, and recent studies have shown that its dynamical behavior is quite different from the normal mode molecules both from the classical[30] and the quantum[4] aspects. Classically, for the normal mode molecules, the normal modes of vibrations are the main modes of their vibrations. This makes the differences in the phase space structure. From the quantum aspects, the dynamical entanglement also shows different characters from that of the local mode molecules.[5] A meaningful work is therefore to investigate the dynamical difference and the relationship between these two types of triatomic molecules, and the study could give us an entire picture of the intramolecular dynamics of the small molecules. The bend vibration in a triatomic system is also important, which has a significant influence on the IVR and the intramolecular chaos. The U(4) algebraic Hamiltonian can also be employed to discuss the influence of the molecular bending vibrations. On the other hand, the classical potential energy surface and the force constants of the tetratomic molecules have also been studied under the U(4) algebraic framework,[56] which means that the method in this paper can be expanded to the tetratomic molecules. These studies are in process.

Acknowledgement

We thank Tao Jia for his contributions to the initial stages of this work.

References

[1] Fujisaki H, Miyadera T and Tanaka A 2003 *Phys. Rev.* E **67** 066201
[2] Gu S, Deng S, Li Y and Lin H 2004 *Phys. Rev. Lett.* **93** 086402
[3] Yu T and Eberly J H 2009 *Science* **323** 598
[4] Hou X W, Chen J H and Ma Z Q 2006 *Phys. Rev.* A **74** 062513
[5] Liu Y, Zheng Y J, Ren W Y and Ding S L 2008 *Phys. Rev.* A **78** 032523
[6] Milman P and Keller A 2009 *Phys. Rev.* A **79** 052303
[7] Cai J M, Popescu S and Briegel H J 2010 *Phys. Rev.* E **82** 021921
[8] Tesch C M and de Vivie-Riedle R 2002 *Phys. Rev. Lett.* **89** 157901
[9] Zhao M Y and Babikov D 2006 *J. Chem. Phys.* **125** 024105
[10] Diaz A and Jung C 2008 *Mol. Phys.* **106** 787
[11] Huang J and Wu G Z 2007 *Chem. Phys. Lett.* **439** 231
[12] Sako T, Yamanouchi K and Iachello F 2002 *J. Chem. Phys.* **117** 1641
[13] Ezra G S 1998 *Adv. Class. Traj. Meth.* **3** 35
[14] Kellman M E and Tyang V 2007 *Acc. Chem. Res.* **40** 243
[15] Manikandan P, Semparithi A and Keshavamurthy S 2009 *J. Phys. Chem.* A **113** 1717
[16] Jaffé C and Brumer P 1980 *J. Chem. Phys.* **73** 5646

[17] Lu Z M and Kellman M E 1997 *J. Chem. Phys.* **107** 6086
[18] Jung C, Ziemniak E, Carvajal M, Frank A and Lemus R 2001 *Chaos* **11** 464
[19] Farantos S C 2004 *J. Chem. Phys.* **126** 175101
[20] Keshavamurthy S and Ezra G S 1997 *J. Chem. Phys.* **107** 156
[21] Sako T and Yamanouchi K 2001 *J. Chem. Phys.* **114** 9441
[22] Arranz F J, Seidel L, Giralda C G, Benito R M and Borondo F 2010 *Phys. Rev.* E **82** 026201
[23] Davis M J 1985 *J. Chem. Phys.* **83** 1016
[24] Tennyson T and Farantos S C 1985 *Chem. Phys.* **93** 237
[25] Yu J and Wu G Z 2001 *Chem. Phys. Lett.* **343** 375
[26] Safi Z S, Losada J C, Benito R M and Borondo F 2008 *J. Chem. Phys.* **129** 164316
[27] Battisti A, Laplopa R G and Tenenbaum A 2009 *Phys. Rev.* E **79** 046206
[28] Keshavamurthy S 2007 *Int. Rev. Phys. Chem.* **26** 4
[29] Carter D and Brumer P 2007 *J. Chem. Phys.* **126** 124307
[30] Sako T, Yamanouchi K and Iachello F 2000 *J. Chem. Phys.* **113** 7292
[31] Yang S B and Kellman M E 2000 *Phys. Rev.* A **62** 022105
[32] Wang X G, Ghose S, Sanders B C and Hu B 2004 *Phys. Rev.* E **70** 0162176
[33] Ghose S and Sanders B C 2004 *Phys. Rev.* A **70** 062315
[34] Chaudhury S, Smith A, Anderson B E, Ghose S and Jessen P 2009 *Nature* **461** 768
[35] Zhang S H and Jie Q L 2008 *Phys. Rev.* A **77** 012312
[36] SibertIII E L, Reinhardt W P and Hynes J T 1982 *J. Chem. Phys.* **77** 3583
[37] Hutchinson J S, SibertIII E L and Hynes J T 1984 *J. Chem. Phys.* **81** 1314
[38] Zheng Y J and Ding S L 2001 *Phys. Rev.* A **64** 032720
[39] Ding S L and Zheng Y J 1999 *J. Chem. Phys.* **111** 4466
[40] Zheng Y J and Ding S L 2000 *J. Mol. Spectrosco.* **201** 109
[41] Zheng Y J and Ding S L 1999 *Phys. Lett.* A **256** 197
[42] Iachello F and Levine R D 1982 *J. Chem. Phys.* **77** 3046
[43] Iachello F and Oss S 1991 *Phys. Rev. Lett.* **66** 2976
[44] Frank A, Lemus R, Bijke R, Pérez-Bernal F and Arias J M 1996 *Ann. Phys.* **252** 211
[45] Iachello F and Truini P 1999 *Ann. Phys.* **276** 120
[46] Feng H R, Liu Y, Zheng Y J, Ren W Y and Ding S L 2007 *Phys. Rev.* A **75** 063417
[47] Zheng Y 2010 *Laser Pulse Phenomena and Applications* (New York: INTECH)
[48] Gilmore R 1981 *Catastrophe Theory for Scientists and Engineers* (New York: Dover Publications)
[49] Zheng Y J and Ding S L 1999 *Chem. Phys.* **247** 225
[50] Zheng Y J and Ding S L 2000 *J. Math. Chem.* **28** 193
[51] Zheng Y J and Ding S L 2008 *Int. J. Quantum. Chem.* **108** 1059
[52] Zheng Y J and Ding S L 2000 *Chem. Phys.* **255** 217
[53] Wilson E B Jr, Decius J C and Cross P C 1955 *Molecular Vibrations* (New York: Van Nostrand)
[54] Zaslavsky G M 2007 *The Physics of Chaos in Hamiltonian Systems* (London: Imperical College Press)
[55] Chirikov B V 1979 *Phys. Rep.* **52** 263
[56] Wang X Y and Ding S L 2004 *Chem. Phys.* **297** 111